7th International Conference on Modelling and Simulation in Nuclear Science and Engineering (7ICMSNSE)
Ottawa Marriott Hotel, Ottawa, Ontario, Canada, October 18-21, 2015

7ICMSNSE-72

A Mesh-Free Method for Approximate Solution of Neutron Transport Equation

D. Altiparmakov
CNL Retiree, Ontario, Canada
dimitar@bell.net

Abstract

This paper presents a new method for approximate solution of the multigroup neutron transport equation. The R-function theory is applied to describe the geometric shape of material regions analytically. Resulting formulae form a basis for a mesh-free approximation of the spatial neutron flux distribution. The method of moments is applied to transform the integral transport equation into a system of linear algebraic equations. Calculations of characteristic two-dimensional CANDU lattice problems show that the method is capable of accurate modeling of the neutron transport with a significant reduction of the number of unknowns compared to standard mesh-based approximations.

Keywords: Neutron Transport, Integral Transport Equation, Mesh-Free Approximation.

1. Introduction

A common objective of deterministic transport methods based on the integro-differential form of neutron transport equation is to approximate the solution with a set of trial functions from a less restrictive class of functions than the class of functions to which the exact solution belongs. This approach is mainly due to the inability of conventional numerical mathematics to handle complex spatial domains on a whole. Instead, such a domain is usually subdivided into a number of subdomains of simple geometric shapes (triangles, rectangles, etc.), to each of which a classical approximation (finite difference, finite element, etc.) could be applied. A benefit of using the integral form of the transport equation is that the approximate solution can be sought in a much less restrictive class of functions than the class of approximate solution of the integro-differential transport equation. It consists of the class of square-integrable functions that allows a large degree of freedom in the choice of trial functions. The simplest form is a constant value throughout each subdomain as used in the collision probability method. By lessening the requirements on trial functions, however, the number of degrees of freedom (unknown coefficients) of the approximate solution may increase significantly. Despite the tremendous capabilities of today's computers, this is still a severe limitation in transport calculation of large heterogeneous systems.

The R-Function Theory [1], [2], [3] is a powerful tool to address the geometric part of the problem in various scientific and engineering disciplines. Using R-functions one can easily construct an analytical, continuous and differentiable function that describes the boundary of a semi-analytic object, i.e., a complex spatial domain the boundary of which consist of parts of analytic surfaces. In this way, the geometric information can be *a priori* and analytically incorporated in the approximate solution of a boundary problem. Accordingly, the R-function

method has been efficiently applied to approximate solution of heat transfer, electrostatics, theory of plates, and other elliptic boundary value problems [3], including the neutron diffusion [4], [5], solid modelling for Monte Carlo calculations [6], analytical modelling of a spiral inflector [7], as well analytical representation of the ZED-2 reactor geometry [8].

Section 2 presents a mesh-free approximation of the spatial distribution of the scalar neutron flux. The trial functions are specified according to the geometric shape of material regions by means of the R-function theory. The method of moments is applied to transform the integral neutron transport equation into a set of linear algebraic equations and determine the unknown coefficients. Section 3 presents the results of calculations of a set of CANDU related two-dimensional test problems. To assess the accuracy of the solution, the mesh-free results are compared with reference Monte Carlo results obtained by the MCNP5 code [9] Version 1.40. On the other hand, comparisons with collision probability calculations, carried out with the lattice cell code WIMS-AECL [10], are given to get an impression about the reduction of the number of unknowns.

2. Theory

The spatial distribution of the scalar neutron flux is a continuous function over the space and differentiable within each material region so that discontinuities of the first derivative occur only at interface boundaries. A mesh-free approximation of such a function is presented in what follows.

2.1 Decomposition of spatial flux distribution

To explain the basic idea of the method, consider a two-region reactor model in one-dimensional geometry. Denote by $V_1, V_2,$ and $V_0 = V_1 \cup V_2$ the spatial domains of the core, reflector, and entire reactor, respectively. They are bounded by the interface boundary $\partial V_{1,2}$ between the core and reflector, and the outer reactor boundary ∂V_0. Accordingly, the boundaries of spatial domains of the core and reflector (V_1 and V_2) are $\partial V_1 = \partial V_{1,2}$ and $\partial V_2 = \partial V_0 \cup \partial V_{1,2}$. Suppose the scalar flux $\varphi(\boldsymbol{r})$ in a thermal group has a shape as shown in Figure 1.a.

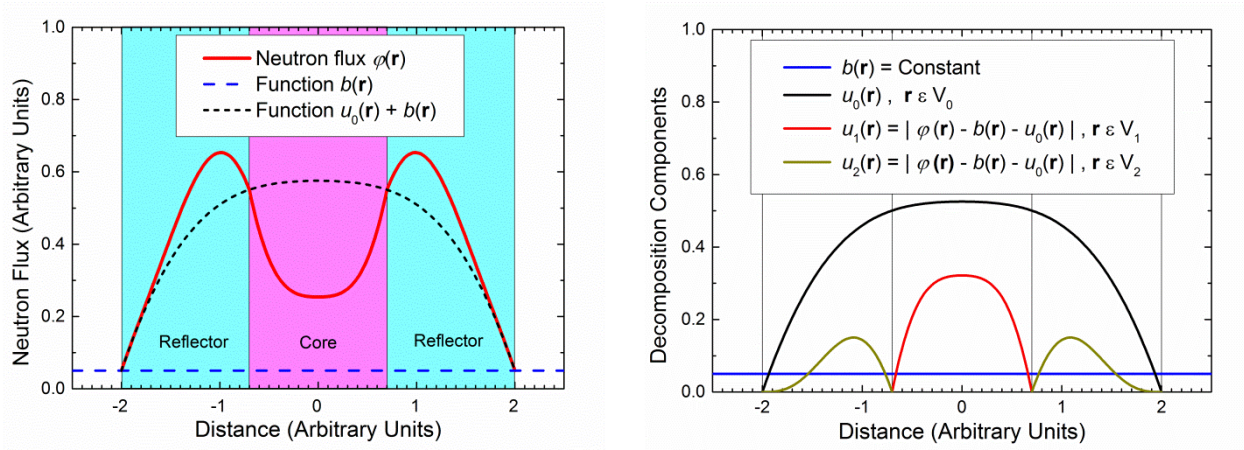

a) Scalar flux and decomposition functions b) Decomposition components

Figure 1 Spatial flux decomposition in a two-region reactor model

Denote by $b(\boldsymbol{r})$ a smooth positive function that is equal to the neutron flux at the outer (vacuum) boundary, i.e., $b(\boldsymbol{r}_0) = \varphi(\boldsymbol{r}_0),\ \boldsymbol{r}_0 \in \partial V_0$. In the particular case of a symmetric reactor model in one-dimensional geometry, as considered here, the function $b(\boldsymbol{r})$ may be represented as a constant. Thus, the problem reduces now to determination of the function $\varphi(\boldsymbol{r}) - b(\boldsymbol{r})$ that is equal to zero at the outer boundary.

As a next step of the flux decomposition, denote by $u_0(\boldsymbol{r})$ a smooth positive function that is equal to $\varphi(\boldsymbol{r}) - b(\boldsymbol{r})$ at both boundaries ∂V_0 and $\partial V_{1,2}$ as shown in Figure 1.a. Consider the properties of the function $f(\boldsymbol{r}) = \varphi(\boldsymbol{r}) - b(\boldsymbol{r}) - u_0(\boldsymbol{r})$. In region V_1 it is a smooth negative function that vanishes at the boundary ∂V_1. Similarly, in region V_2 it is also a smooth but positive function that vanishes at ∂V_2. Instead of a single function $f(\boldsymbol{r})$, one may specify two continuous positive functions $u_1(\boldsymbol{r})$ and $u_2(\boldsymbol{r})$ as follows:

$$u_1(\boldsymbol{r}) = \begin{cases} |\varphi(\boldsymbol{r}) - b(\boldsymbol{r}) - u_0(\boldsymbol{r})|\,, & \boldsymbol{r} \in V_1 \\ 0\,, & \boldsymbol{r} \notin V_1 \end{cases}, \quad u_2(\boldsymbol{r}) = \begin{cases} |\varphi(\boldsymbol{r}) - b(\boldsymbol{r}) - u_0(\boldsymbol{r})|\,, & \boldsymbol{r} \in V_2 \\ 0\,, & \boldsymbol{r} \notin V_2 \end{cases} \quad (1)$$

Hence, the neutron flux distribution can be represented as a linear combination of the functions $u_0(\boldsymbol{r}),\ u_1(\boldsymbol{r})$ and $u_2(\boldsymbol{r})$ plus the boundary term $b(\boldsymbol{r})$, i.e.,

$$\varphi(\boldsymbol{r}) = b(\boldsymbol{r}) + \sum_{i=0}^{2} s_i\, u_i(\boldsymbol{r}) \quad (2)$$

where the coefficients s_i specify the sign (+1 or –1) of the related contribution. Note that, as shown in Figure 1.b, each function $u_i(\boldsymbol{r})$ is a smooth positive function within the related domain V_i $(i = 0,1,2)$ and equal to zero on its boundary ∂V_i and everywhere else. In a general case of a multi-region problem, the summation in equation (2) should be carried out over all material regions as well as a number of spatial domains that represent unions of two or more material regions up to the spatial domain of the entire reactor model.

2.2 Approximate solution of two-region problem

According to equation (2), one may look for an approximate solution of the two-region problem in the following form:

$$\varphi(\boldsymbol{r}) \approx c(\boldsymbol{r}) + \sum_{i=0}^{2} \sum_{j=1}^{n_i} \varphi_{i,j} \cdot f_{i,j}(\boldsymbol{r}) \quad (3)$$

where $c(\boldsymbol{r})$ is an approximation of the boundary term $b(\boldsymbol{r})$, $\varphi_{i,j}$ are unknown coefficients to be determined, and $f_{i,j}(\boldsymbol{r})$ are basis functions of a set of n_i functions intended to approximate the corresponding functions $u_i(\boldsymbol{r})$. Accordingly, each function $f_{i,j}(\boldsymbol{r})$ is a smooth positive function within the related domain V_i and vanishes on its boundary ∂V_i and outside V_i.

The R-function theory provides a simple mathematical apparatus to construct a continuous and differentiable function $\omega(\boldsymbol{r})$ for an arbitrary semi-analytic domain in order to describe the domain analytically as follows:

$$\omega(\boldsymbol{r})\begin{cases} >0\,, & \boldsymbol{r}\in V \\ =0\,, & \boldsymbol{r}\in \partial V \\ <0\,, & \boldsymbol{r}\notin V\cup\partial V \end{cases} \tag{4}$$

Having specified a function $\omega_i(\boldsymbol{r})$ for each domain V_i $(i = 0,1,2)$, one can easily construct functions $\omega_i^+(\boldsymbol{r})$ that satisfy the requirements of the approximate solution (3) as follows:

$$\omega_i^+(\boldsymbol{r}) = \frac{1}{2}(\omega_i(\boldsymbol{r}) + |\omega_i(\boldsymbol{r})|) = \begin{cases} >0\,, & \boldsymbol{r}\in V_i \\ 0\,, & \boldsymbol{r}\notin V_i \end{cases} \tag{5}$$

To get a set of functions $f_{i,j}(\boldsymbol{r})$ for each domain V_i, one may either apply a set of power function $(\omega_i^+)^j$ or a product of ω_i^+ with a set of continuous positive functions, or both.

2.3 Approximate solution of a CANDU lattice cell model

Consider an infinite lattice of a periodically repeating lattice cell, for instance the 37-element CANDU lattice cell as depicted in Figure 2.a. The fuel (natural uranium) is arranged in fuel bundles that consist of a central pin surrounded with three rings of fuel pins. There are six pins in the inner ring, 12 pins in the middle ring and 18 pins in the outer ring. Fuel bundles are loaded in a pressure tube surrounded by air gap and a calandria tube to physically separate the moderator from the coolant. Owing to the physical properties of the problem, the approximate solution does not necessarily need to treat explicitly each material region. For instance, optically thin regions, such as the cladding and the gap, do not affect significantly the flux distribution. They can be accounted for by using a union of an optically thin domain and another adjacent material region. Suppose that functions $\omega_i(\boldsymbol{r})$ are constructed for the following spatial domains:

ω_1 All fuel regions
ω_2 Coolant and cladding regions
ω_3 Fuel channel interior (everything inside the inner boundary of the pressure tube)
ω_4 Fuel channel exterior (everything outside the inner boundary of the pressure tube)
ω_5 Pressure and calandria tubes including the air gap between them
ω_6 Calandria tube interior (everything inside the outer boundary of the calandria tube)
ω_7 Moderator

The above functions $\omega_i(\boldsymbol{r})$ must obey the same periodicity as the infinite reactor lattice itself. Details about their construction can be found in Reference [8]. The following set of $N = 15$ basis functions was used for the calculation of single cell test problems presented in Section 3:

$$\{f_n\} = \begin{Bmatrix} \omega_1^+\,, & \omega_1^+\omega_3^+\,, & \omega_2^+\,, & \omega_2^+\omega_3^+\,, & \omega_3^+\,, & (\omega_3^+)^2, & (\omega_3^+)^3, \\ \omega_4^+\,, & (\omega_4^+)^2, & \omega_5^+\,, & \omega_6^+\,, & \omega_7^+\,, & (\omega_7^+)^2, & (\omega_7^+)^3, & (\omega_7^+)^4 \end{Bmatrix} \tag{6}$$

Here, a single function is used for certain regions (V_5 and V_6), while two or more functions are necessary for spatial domains of large flux variations (fuel, coolant, fuel channel and moderator). Also, all basis functions are assembled in a single set of functions, instead of separate sets for each spatial domain as used in equation (3). Accordingly, the approximate solution can be represented in the following form, where the boundary term is omitted since there is no vacuum boundary in the infinite lattice model:

$$\varphi(\boldsymbol{r}) = \sum_{n=1}^{N} \varphi_n f_n(\boldsymbol{r}) \tag{7}$$

2.4 Determination of unknown coefficients

For a given energy group, the integral neutron transport equation can be written in the following general form, where the group index is omitted for simplicity:

$$\varphi(\boldsymbol{r}) = \int_V d^3r' K(\boldsymbol{r}, \boldsymbol{r}') [\, \Sigma_s(\boldsymbol{r})\, \varphi(\boldsymbol{r}) + s(\boldsymbol{r})] \tag{8}$$

V denotes the spatial domain where neutron transport occurs (entire three-dimensional space for the infinite lattice model or a finite domain of a reactor model), $\boldsymbol{r} = \{x, y, z\}$ and $\boldsymbol{r}' = \{x', y', z'\}$ are radius vectors, $\Sigma_s(\boldsymbol{r})$ is the scattering cross section, and $s(\boldsymbol{r})$ is the scattering and fission source in considered group. The explicit shape of the integral kernel $K(\boldsymbol{r}, \boldsymbol{r}')$ is as follows:

$$K(\boldsymbol{r}, \boldsymbol{r}') = \frac{exp[-\tau(\boldsymbol{r}, \boldsymbol{r}')]}{4\pi|\boldsymbol{r} - \boldsymbol{r}'|^2} \quad , \quad \tau(\boldsymbol{r}, \boldsymbol{r}') = \int_0^{|\boldsymbol{r}-\boldsymbol{r}'|} \Sigma_t\, (\boldsymbol{r} - \xi \frac{\boldsymbol{r} - \boldsymbol{r}'}{|\boldsymbol{r} - \boldsymbol{r}'|}) d\xi \tag{9}$$

where ξ is the geometrical distance along the direction $\boldsymbol{\Omega} = (\boldsymbol{r} - \boldsymbol{r}')/|\boldsymbol{r} - \boldsymbol{r}'|$.

The neutron source $s(\boldsymbol{r})$ can be expanded over the same set of basis functions as the neutron flux presented in equation (7). Denote by s_n the corresponding expansion coefficients. The method of moments can be applied to determine the unknown coefficients. To this end, the neutron flux and neutron source approximations are substituted into Eq. (8), which is then multiplied by a basis function $f_m(\boldsymbol{r})$ and integrated over a spatial domain V^*, which is equal to a repeating part of the infinite lattice model or the spatial domain V of the full reactor model, i.e.,

$$\int_{V^*} d^3r\, f_m(\boldsymbol{r}) \sum_{n=1}^{N} \varphi_n f_n(\boldsymbol{r}) = \int_{V^*} d^3r\, f_m(\boldsymbol{r}) \int_V d^3r' K(\boldsymbol{r}, \boldsymbol{r}') \sum_{n=1}^{N} \varphi_n f_n(\boldsymbol{r}) [\, \Sigma_s(\boldsymbol{r})\, \varphi_n + s_n)] \tag{10}$$

Repeating this procedure for each basis function $f_m(\boldsymbol{r})$, $m = 1,2, \ldots N$, one gets a system of N linear equations that determine the unknown coefficients φ_n, $n = 1,2, \ldots N$:

$$\sum_{n=1}^{N} a_{m,n} \varphi_n = \sum_{n=1}^{N} b_{m,n} \varphi_n + \sum_{n=1}^{N} c_{m,n}\, s_n \quad , \quad m = 1,2, \ldots N \tag{11}$$

where the coefficients $a_{m,n}$, $b_{m,n}$ and $c_{m,n}$ are specified as follows:

$$a_{m,n} = \int_{V^*} d^3r\, f_m(\boldsymbol{r})\, f_n(\boldsymbol{r}) \tag{12}$$

$$b_{m,n} = \int_{V^*} d^3r \int_V d^3r' K(\boldsymbol{r}, \boldsymbol{r}') f_m(\boldsymbol{r}) f_n(\boldsymbol{r}')\, \Sigma_s(\boldsymbol{r}') \tag{13}$$

$$c_{m,n} = \int_{V^*} d^3r \int_V d^3r' K(\boldsymbol{r}, \boldsymbol{r}') f_m(\boldsymbol{r}) f_n(\boldsymbol{r}') \tag{14}$$

3. Results

A prototype computer program has been written in Fortran 95 to test the method. The code includes a number of modules of the WIMS-AECL code to carry out the following tasks: read input data, retrieve library data, prepare macroscopic cross sections, perform resonance self-shielding, and do the ray tracing for numerical integration of the necessary space integrals. Thus, the prototype code uses identical multigroup cross sections as the WIMS-AECL code.

3.1 Test problems

A set of test problems were specified using the 37-element CANDU lattice cell as the basic element of the models. Figure 2.a shows the geometric model of the 37-element lattice cell, which is used as is by the mesh-free approach without any subdivision except the fuel subdivision for resonance self-shielding. For the sake of comparison with a mesh based approach, Figure 2.b presents the mesh subdivision as used for routine collision probability calculations by the WIMS-AECL code. Three groups of problems were specified as follows:

A. Three single cell models representing infinite lattices of periodically repeating cells:
   1. Lattice cell with fresh fuel at regular operating conditions.
   2. Lattice cell with fresh fuel and voided coolant.
   3. Lattice cell with discharge (burnt) fuel at regular operating conditions.

B. Two checkerboard lattices each of which contains two types of fuel channels as follows:
   1. Cooled and voided fuel channels with fresh fuel.
   2. Fuel channels with fresh and burnt fuel in a checkerboard pattern.

C. Core-reflector interface problem represented by a row of fuelled cells surrounded by two reflector cells. Four cases are considered varying the number of fuelled cells from 2 to 5.

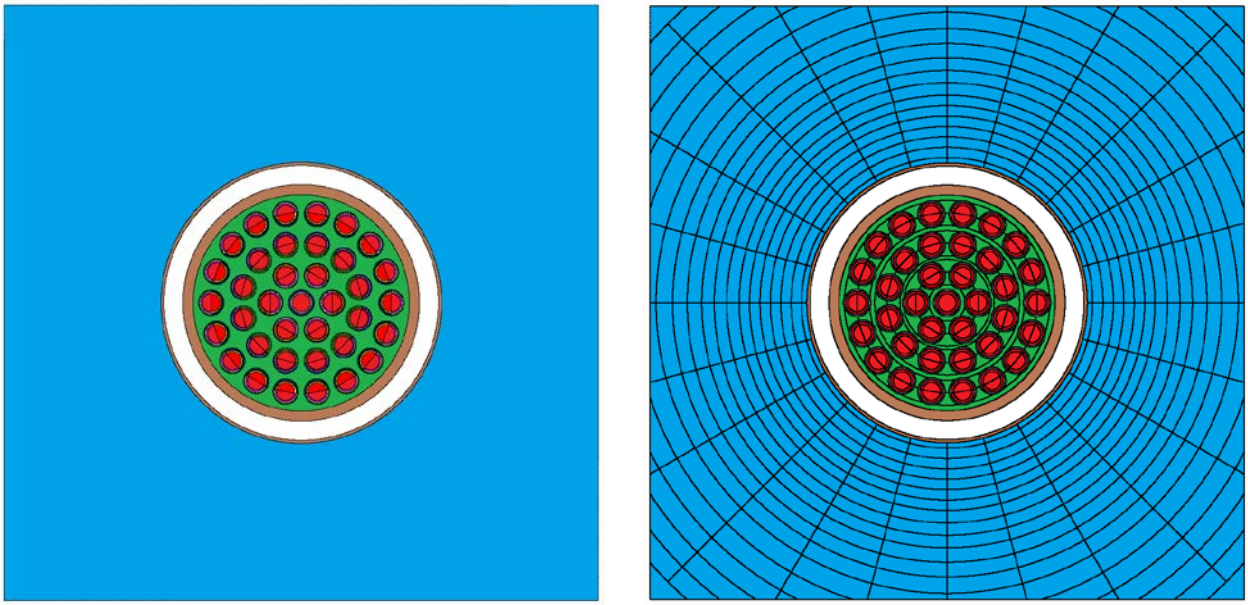

a) Geometric model b) Mesh subdivision

Figure 2 Geometric model and a typical mesh subdivision of 37-element lattice cell

3.2 The shape of spatial flux distribution

The mesh free-approximation produces an approximate solution that is continuous in space and differentiable within each material region. To illustrate the solution shape, Figure 3 shows three-dimensional plots of spatial flux distributions in energy groups 11 and 76 as two characteristic groups (peak flux values of the fast and thermal neutron flux, respectively) of the 89-group approximation. For comparison, Figure 4.a presents a three-dimensional plot of the MCNP-calculated flux distribution in energy group 76. The plots are very similar to each other, except that a granular structure is visible in MCNP results. It is due to the uncertainties in the mesh flux tallies, which is still visible despite one billion active histories were used in this calculation. In contrast to the continuous solution of the mesh-free approximation, the collision probability method produces a step-wise approximation of the neutron flux as presented in Figure 4.b. The visual impression is quite different from both mesh-free and MCNP results.

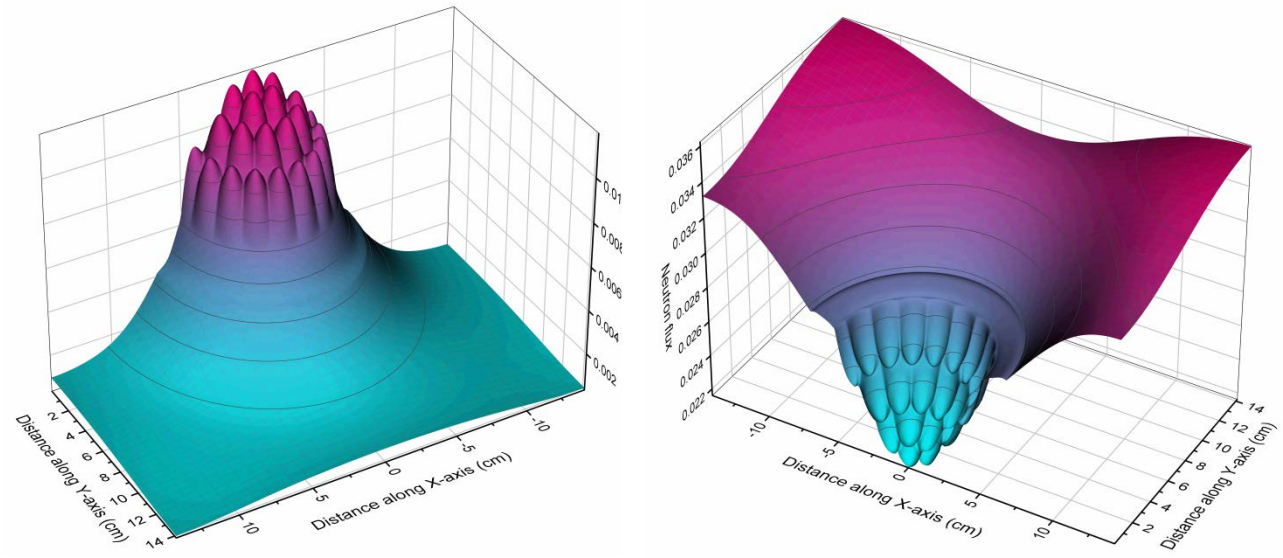

a) Neutron flux in energy group 11 b) Neutron flux in energy group 76

Figure 3 Mesh-free approximation of neutron flux distribution in two characteristic energy groups

3.3 Accuracy of mesh-free approximation

To get an insight into the accuracy of the spatial and energy approximations, 89-group reference MCNP results were obtained for the single-cell test problem. The FMESH option was applied to 89 energy bins having the same structure as the 89-group library of WIMS-AECL in order to get the spatial flux distribution in each energy group as flux tallies on a rectangular mesh of 1mm×1mm size. Figure 5.a shows the root mean square (RMS) values of the uncertainties in mesh flux tallies for each energy group. Three calculations were carried out using 20 million, 100 million, and 1 billion active histories. The results show that 20 million histories produce an average uncertainty of about 2.9% with a maximum value of 10%. Increasing the number of histories to 100 million, the average uncertainty reduces to 1.3% with a maximum of 4.5%. One billion histories are necessary for an average uncertainty of 0.5%.

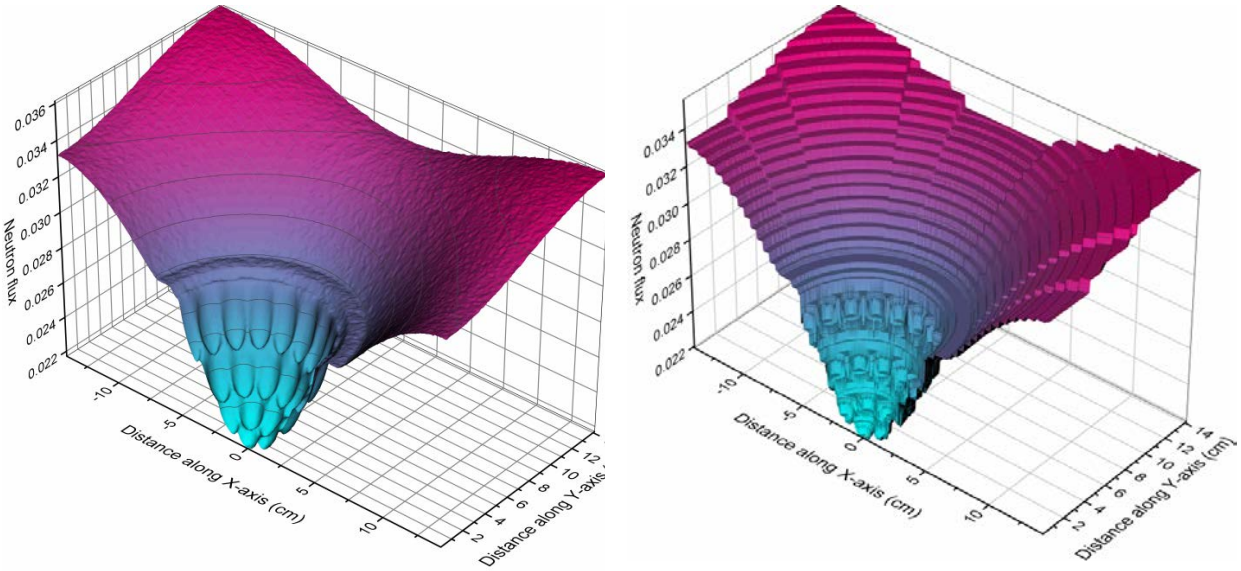

a) MCNP mesh flux tallies b) Collision probability approximation

Figure 4 Monte Carlo and collision probability solutions in energy group 76

Figure 5.b presents the RMS error of the mesh-free approximation. The first group exhibits the maximum error of 15%. In other groups the error varies around 1-2% with a few exceptions where it reaches higher values up to 5%.

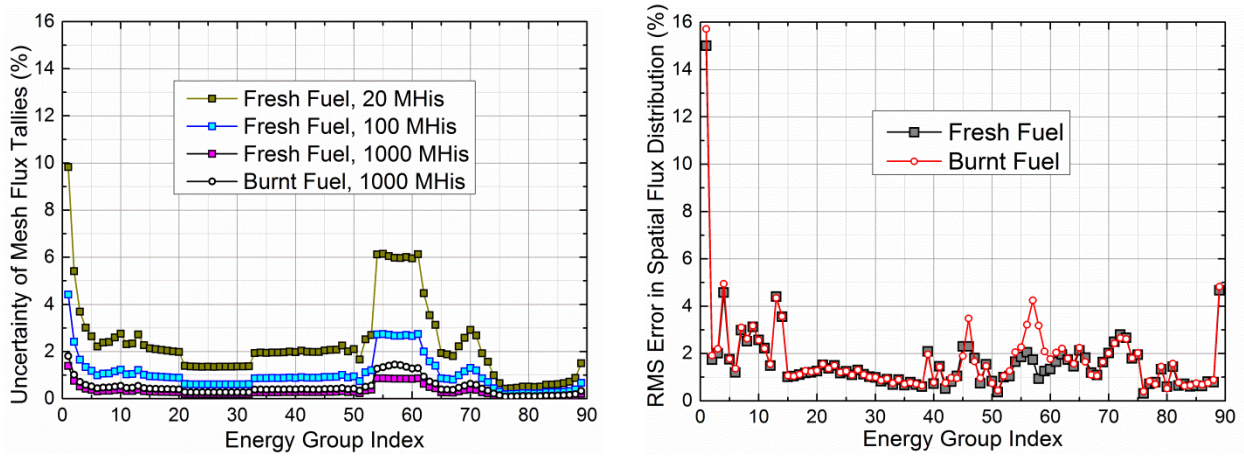

a) Uncertainty of MCNP flux tallies b) RMS error of mesh-free approximation

Figure 5 MCNP uncertainty versus RMS error of mesh-free approximation

As a visual illustration of the agreement/discrepancy between the mesh-free approximation and MCNP results, Figure 6 presents the flux distribution along the central line across the cell of the test problem A.1 as calculated by both methods for a number of selected energy groups. For fast and thermal energy groups (Figure 6.a and Figure 6.d), the results of both methods visually almost coincide with each other. A slight increase of the discrepancy can be observed in the resonance groups (Figure 6.b and Figure 6.c), which is likely due to the resonance self-shielding.

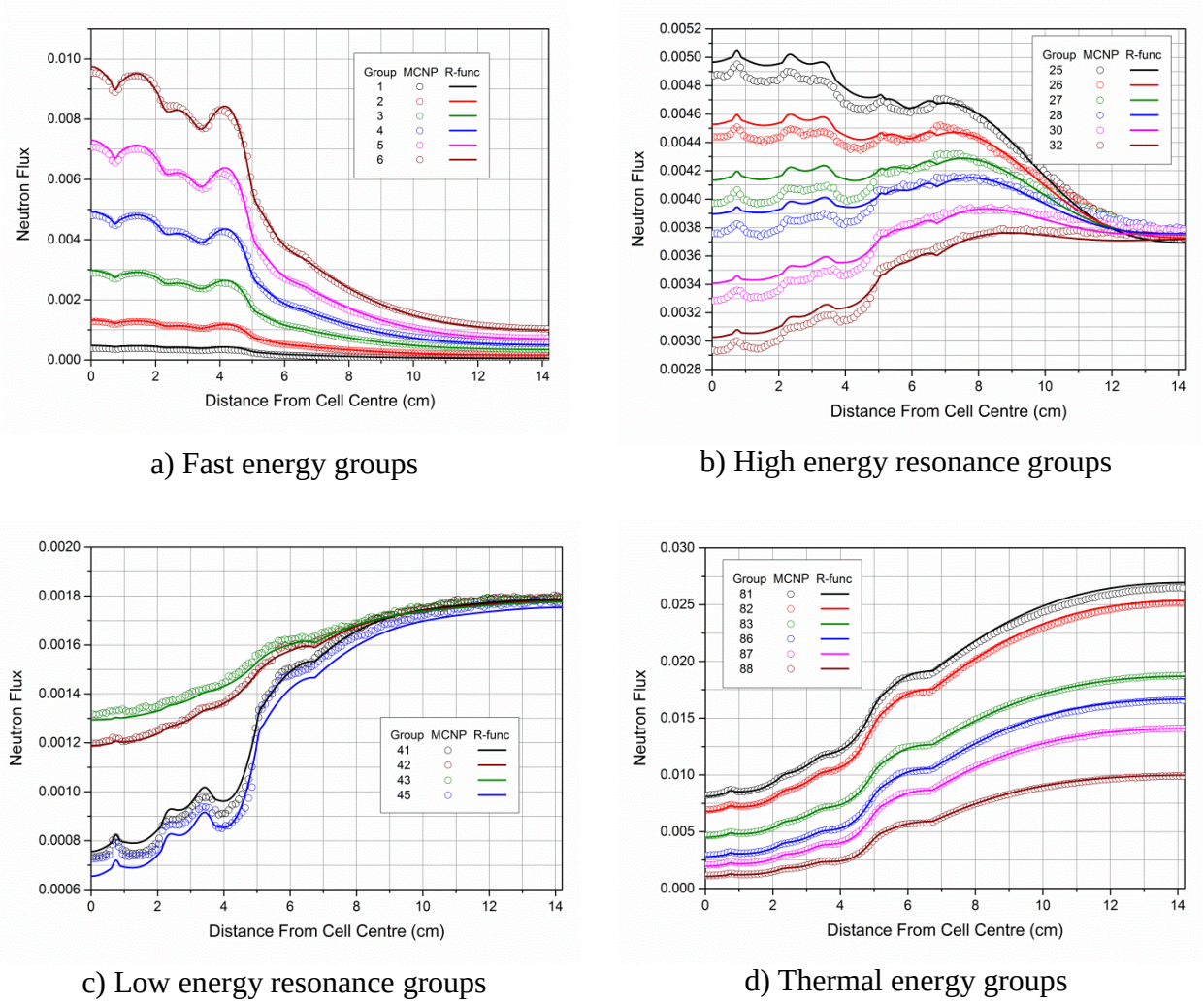

a) Fast energy groups

b) High energy resonance groups

c) Low energy resonance groups

d) Thermal energy groups

Figure 6 Comparison of MCNP mesh flux tallies and mesh-free flux approximation along the central line across the lattice cell for a set of selected energy groups

Due to MCNP5 limits, 89-group mesh flux tallies could not be calculated for multicell test problems B and C. Instead, two-group tallies were used to determine the spatial distribution of the fast and thermal neutron groups, which cover the energy ranges above and below 4 eV, respectively. The neutron flux is normalized to k fission neutrons in entire system, where k stands for the neutron multiplication factor. To illustrate the agreement between mesh-free and MCNP results, Figure 7 shows the fast and thermal neutron fluxes in the checkerboard lattice model of fresh and burnt fuel (test problem B.2). The spatial variation of the two-group flux is given as a function of the x-coordinate (the distance from the y-axis that passes though a cell centre) along two lines, the central line ($y = 0$) and the cell edge line ($y = p/2$, where p stands for the lattice pitch). For the sake of visual clarity, vertical lines show the intersections of the x-z plane with the boundaries of the central fuel pin, a fuel pin of the inner and a fuel pin of the outer ring. The intersections with the outer and inner boundaries of pressure and calandria tubes are also presented. Figure 8 shows the spatial variation of fast and thermal neutron fluxes along two lines of two core-reflector interface models represented by two/three fueled cells and two

reflector cells. The figures show that the results of mesh-free approximation are in very good agreement with MCNP results.

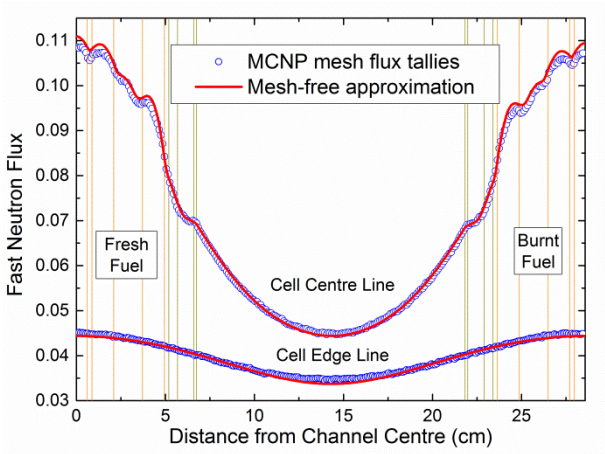

a) Fast neutron flux distribution

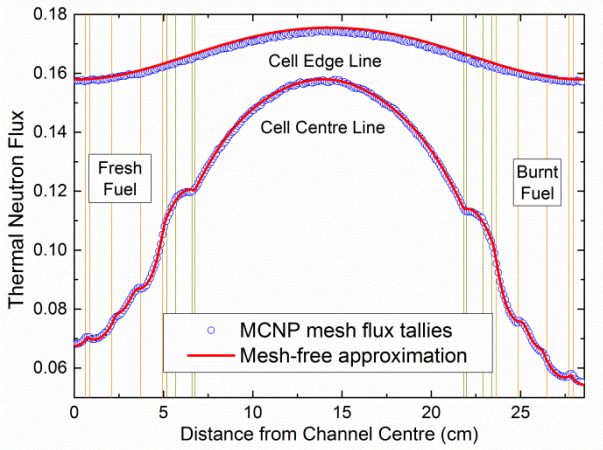

b) Thermal neutron flux distribution

Figure 7 Mesh-free approximation versus MCNP mesh flux tallies in a checkerboard lattice of fresh and burnt fuel channels

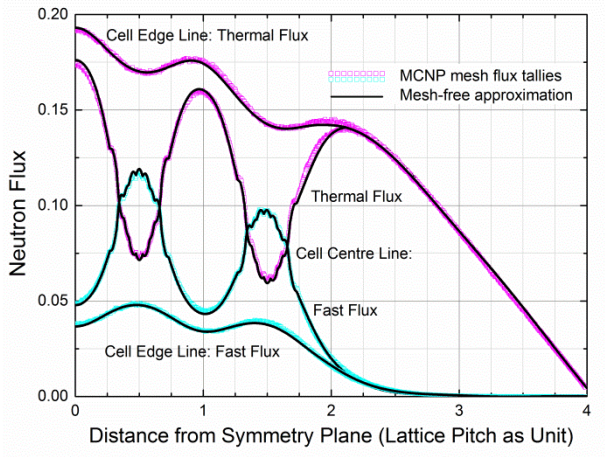

a) Two fuelled cells

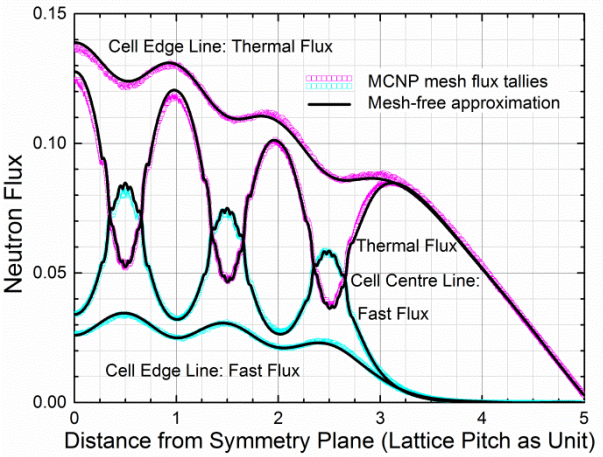

b) Three fuelled cells

Figure 8 Mesh-free approximation versus MCNP mesh flux tallies in two models of the core-reflector interface problem

3.4 Reduction of the number of unknowns

To compare the mesh-free method with a mesh-based approximation, collision probability calculations were carried out with a developmental version of the lattice cell code WIMS-AECL for all test problems considered. Table 1 summarizes the results of the three methods using MCNP values of the neutron multiplication factor as the reference ones. The discrepancy of collision probability results ranges from -0.58 to 0.08 mk, while the mesh-free method produces a slightly smaller discrepancy that ranges from -0.13 to 0.34 mk. The number of unknowns per

group in collision probability calculations varies from 142 to 4702 depending on the test problem considered. For the same test problems, the number of unknowns per group of the mesh-free method varies from 15 to 61. Thus, a significant reduction is achieved by the mesh-free method. Increasing the complexity of the problem, the reduction factor increases from 9.5 for the single-cell problems to 77 for the core-reflector interface model C.4.

Table 1 A summary of the results

Test Case	MCNP			WIMS-AECL				Mesh-free approximation				$\frac{N_{cp}}{N_{mf}}$
	k-inf	σ (mk)	CPU	k-inf	Δk (mk)	N_{cp}	CPU (s)	k-inf	Δk (mk)	N_{mf}	CPU (s)	
A.1	1.11423	±0.01	1 week	1.11431	0.08	142	11	1.11449	0.26	15	47	9.5
A.2	1.13586	±0.04	2 days	1.13534	-0.52	142	12	1.13573	-0.13	15	49	9.5
A.3	0.98544	±0.01	2 weeks	0.98578	0.34	142	17	0.98561	0.17	15	53	9.5
B.1	1.12528	±0.09	13 hours	1.12503	-0.25	284	44	1.12524	-0.04	26	137	10.9
B.2	1.04635	±0.10	44 hours	1.04669	0.34	284	50	1.04664	0.29	26	141	10.9
C.1	1.03149	±0.05	36 hours	1.03170	0.21	2086	135	1.03176	0.27	34	314	61.4
C.2	1.06375	±0.10	8 hours	1.06356	-0.19	2958	280	1.06403	0.28	43	574	68.8
C.3	1.07985	±0.10	8 hours	1.07940	-0.45	3830	493	1.08016	0.31	52	688	73.6
C.4	1.08926	±0.10	8 hours	1.08868	-0.58	4702	846	1.08960	0.34	61	1090	77.1

N_{cp} = Number of unknowns in collision probability solution
N_{mf} = Number of unknowns in mesh-free approximation
N_{cp} / N_{mf} = Reduction factor in the number of unknowns

Compared to the standard collision probability approximation, the mesh-free method applies an additional two-fold numerical integration for the calculation of the space integrals specified by equations (12) – (14). Thus, the calculation of matrix coefficients is computationally more intensive than the calculation of collision probabilities, so that an increase in related computing time should be expected. This component of the total computing time is dominant in collision probability calculation of small-size problems. Increasing the problem size, however, the solution of the system of linear equations becomes a dominant component of the total computing time. On the other hand, due to the significant reduction of the number of unknowns, the solution time of the mesh-free method is very fast. Accordingly, Table 1 shows that the mesh-free computing time of the single-cell cases is about 4 times longer than the WIMS-AECL computing time. However, the difference in CPU times decreases with the increase of the problem complexity, so that for the C.4 case the CPU time ratio falls down to ~1.3. Regarding the timing results, it is worth mentioning that the version of the WIMS-AECL code used here is highly optimized concerning the computing speed, while mesh-free calculations were carried out with a prototype code without substantial attempts to speed up the calculations.

4. Conclusion

A mesh-free method is developed for approximate solution of the multigroup neutron transport equation. The approximate solution is presented as a linear combination of analytic functions that are specified according to the geometric properties of the problem and constructed by means of the R-function theory. Owing to the analytic form, the solution is convenient for visual presentation and, as such, facilitates the analysis of the spatial flux behaviour in various physics phenomena. The results of calculations of three sets of characteristic test problems show that the

method is capable of accurate modelling of the neutron transport in CANDU related physics phenomena. The results are in a very good agreement with reference Monte Carlo calculations. Compared to the standard collision probability approximation, the same accuracy is achieved with a significant reduction of the number of unknowns. The reduction factors ranges from 9 to 77, depending on the test problem considered. It increases with the complexity of the problem so that the higher the number of unknowns in the mesh-based collision probability solution, the higher is the reduction factor of the mesh-free approximation.

5. Acknowledgment

This work was performed at Canadian Nuclear Laboratories – CNL (formerly Atomic Energy of Canada Limited – AECL) within the framework of a Candu Owners Group – COG project. The author uses this opportunity to express his thanks to the CNL management and COG Physics Group members for their support. Special thanks are due to Sharon Pfeiffer for her assistance in MCNP calculations.

6. References

[1] V.L. Rvachev, "On analytical description of some geometric objects", *Reports (Doklady) of Academy of Sciences*, USSR, Vol. 153, 1963, pp, 765–768.

[2] V.L. Rvachev and V.A. Rvachev, "Nonclassical methods of approximation theory in boundary values problems", Izd. Naukova Dumka Kiev, 1979. In Russian.

[3] V.L. Rvachev, "R-function theory and some of its applications", Izd. Naukova Dumka, Kiev, 1982. In Russian.

[4] D.V. Altiparmakov, "Nested element method in multidimensional neutron diffusion calculations", Proc. CNS/ANS Int. Conference on Numerical Methods in Nuclear Engineering, Montreal, Canada, 1983, September 6-9, Vol. 1, pp. 327-347.

[5] D.V. Altiparmakov, "On trial functions in the nested element method", *Nucl. Sci. Eng.*, Vol. 92, No. 2, 1986, pp.330-337.

[6] D.V. Altiparmakov and P. Belicev, "An efficiency study of the R-function method applied as solid modeler for Monte Carlo calculations", *Progress in Nuclear Energy*, Vol. 24, No. 1-3, 1990, pp. 77-88.

[7] P. Belicev and D.V. Altiparmakov, "An efficient electric field approximation for spiral inflector calculations", *Nuclear Instruments and Methods in Physics Research – A*, Vol. 456, No. 3, 2001, pp. 177-189.

[8] D. Altiparmakov, "Analytical representation of ZED-2 reactor geometry by means of the R-function method", *AECL Nuclear Review*, Vol. 2, No. 1, 2013, pp. 27-37.

[9] X-5 Monte Carlo Team, "MCNP – A general N-particle transport code, Version 5 – Volume I; Overview and Theory", LA-UR-03-1987, Los Alamos National Laboratory, 2005.

[10] D. Altiparmakov, "New capabilities of the lattice code WIMS-AECL", Proceedings of PHYSOR 2008, the International Conference on Reactor Physics, Nuclear Power: A Sustainable Resource", Interlaken, Switzerland, September 14-19, 2008, Paper 246.